Sensor and Simulation Notes

Note 489

April 2004

A High-Voltage UWB Coupled-Line Directional Coupler

Lanney M. Atchley, Everett G. Farr, and Donald E. Ellibee
Farr Research, Inc.

Dean I. Lawry
Air Force Research Laboratory, Directed Energy Directorate

Abstract

The simplest method of building Ultra-Wideband (UWB) radar systems requires two antennas, one each for transmission and reception. To save space, it would be preferable to use a single antenna, so a UWB, high-voltage directional coupler is needed. In support of that goal, we develop here coupled-line directional couplers. We begin by describing the time-domain theory of operation of such couplers, and we optimize the impedances for maximum return signal. We then design, build and test two versions of high-voltage coupled-line directional couplers. We incorporate the directional couplers into a low-voltage UWB radar system, and we observe scattering back from a corner reflector. We identify possible improvements to the directional couplers and the UWB radar system.

CONTENTS

1. Introduction

Ultra-Wideband (UWB) radar systems have the potential for identifying and locating non-cooperative targets. However, such systems normally require two separate antennas, one each for transmission and reception. Because each antenna may be large, it could be challenging to mount both of them onto a single vehicle. It would be preferable to use a single antenna for both transmission and reception.

To build a UWB radar that uses a single antenna, a key component is a UWB high-voltage directional coupler. Baum has recently proposed the use of a coupled-line directional coupler in [1]. Coupled lines have already been used in directional couplers at low voltages for narrowband applications [2]. However, such devices have never been used at high voltages or in UWB applications. We demonstrate here the feasibility of high-voltage UWB directional couplers. Our design goals were a peak voltage of 50 kV and a bandwidth of over 2 GHz.

Some alternative techniques for using a single antenna in a UWB radar system were demonstrated by Piette in [3]. These techniques used either a GaAs single-pole double-throw switch or an array of power splitters. But these approaches either operated at too low a voltage or had too high an attenuation for our application.

We begin by predicting the performance of coupled-line directional couplers in the time domain. We calculate the voltages at all four ports of the coupler as a function of the even-mode and odd-mode impedances. We then optimize the impedances to maximize the coupling in transmission and reflection.

Next, we built and tested two high-voltage directional coupler designs: a traditional asymmetrical design and a symmetrical design. Both designs performed about as expected, but the symmetrical model had marginally fewer impedance discontinuities and thus somewhat better performance. We identify some shortcomings in our initial designs and suggest improvements for a deployable prototype.

Finally, we tested the directional couplers in a variety of low-voltage UWB radar configurations, and we successfully identified radar backscatter in the received signal. We experimented with a number of sources, finding one that worked well and two that did not. While experimenting with sources, we developed an impulse forming network (IFN) built by embedding a blocking capacitor into the center conductor of a coaxial cable. The output of this device was the derivative of the driving source waveform.

We begin by describing how a directional coupler can fit into a UWB radar system.

2. UWB Radar System Description

The simplest way to design an Ultra-Wideband (UWB) radar system is to use two separate antennas for transmission and reception. This may be a disadvantage if aperture area is limited, so a directional coupler has been proposed as one method to distinguish between the transmitted and returned signal. We develop here the design equations for a symmetric coupled-line directional coupler. We consider here only transmission line configurations with symmetrical impedance matrices, and with the two center conductors closely spaced. We do so because we see a need for strong coupling.

To understand the need for a directional coupler, we provide a diagram of a UWB radar system with a single antenna.. The diagram, shown in Figure 2.1, shows a UWB source (Port 1) connected to an antenna (Port 2) through a directional coupler of length ℓ. When a signal is received back from a target in Port 2, an exact replica of the received signal is coupled into Port 4, where it is detected by an oscilloscope. The signal at Port 4 is an exact replica for a time equal to the round-trip transit time of the coupler [1], or $2\ell\sqrt{\varepsilon_r}\,/\,c$. A signal conditioner and limiter circuit protect the oscilloscope from spurious high-voltage signal that can leak through the coupler due to its finite directivity.

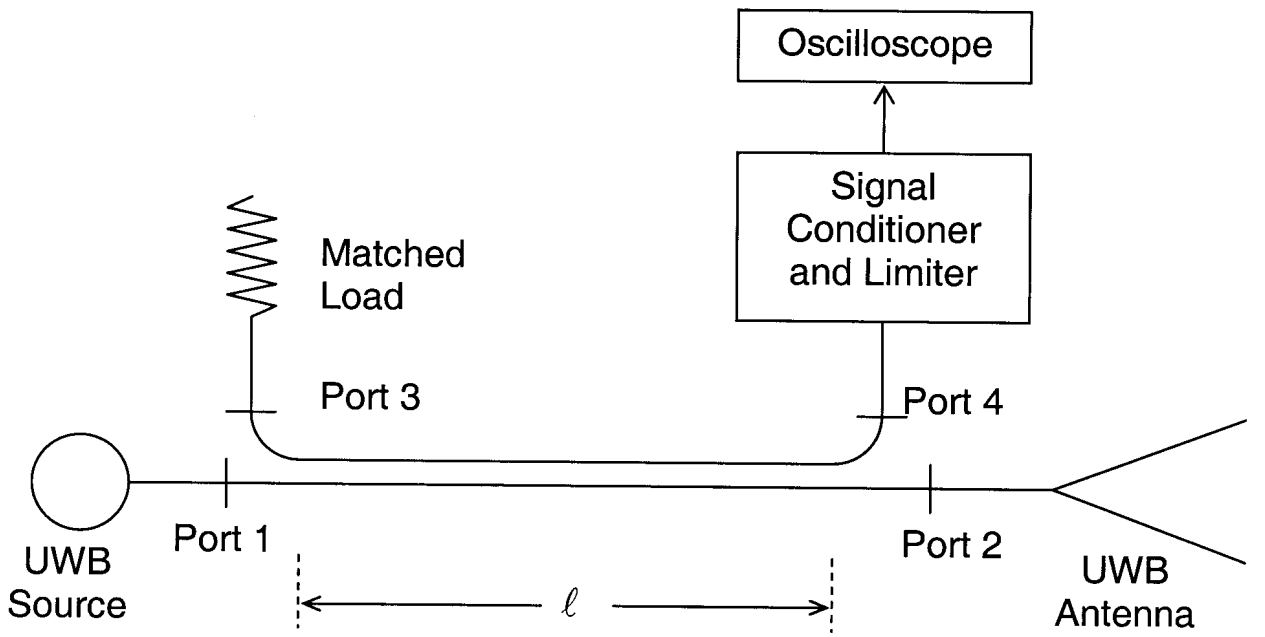

Figure 2.1. Generic UWB Radar system with single antenna.

To analyze the directional coupler, we note that the coupled transmission lines form an odd- and even-mode pair of lines, as shown in Figure 2.2. These lines have an impedance of Z_{0e} and Z_{0o}, which are related by the expression

$$Z_0 = \sqrt{Z_{0e}\, Z_{0o}} \tag{2.1}$$

where Z_0 is the 50-ohm output impedance at each of the ports. If the transmission lines are composed of round conductors between two plates (suitable for high-voltages), the even and odd-mode impedances may be calculated by analyzing the two transmission lines with charges as shown in Figure 2.2. To calculate the even-mode and odd-mode impedances, we solve a 2-dimensional Laplace's equation either analytically or numerically, using Finite Element Analysis.

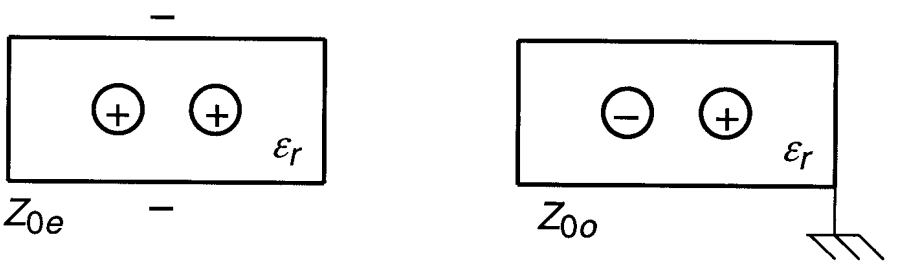

Figure 2.2. Cross section of even mode (left) and odd-mode (right) transmission lines.

We proceed now to a calculation of the voltages into all four ports of a coupled-line directional coupler. We then optimize the choice of impedance, to obtain the maximum voltage into the scope.

3. Directional Coupler Theory

We begin with the coupler shown in Figure 3.1, consisting of two parallel transmission lines, with four ports. Port 1 is driven by a step-function voltage $V_0u(t)$ and signal is conveyed to the through port, Port 2. The signal couples into Port 3, and ideally Port 4 will receive no signal. All four ports have a load impedance of Z_0 = 50 Ω. Because we are considering only the time domain response, we are concerned only with the initial signal seen by each port. This signal lasts for one round-trip transit time of the coupler. We assume that the transmission line is surrounded by a uniform dielectric material, so the propagation velocity of the even and odd modes are the same.

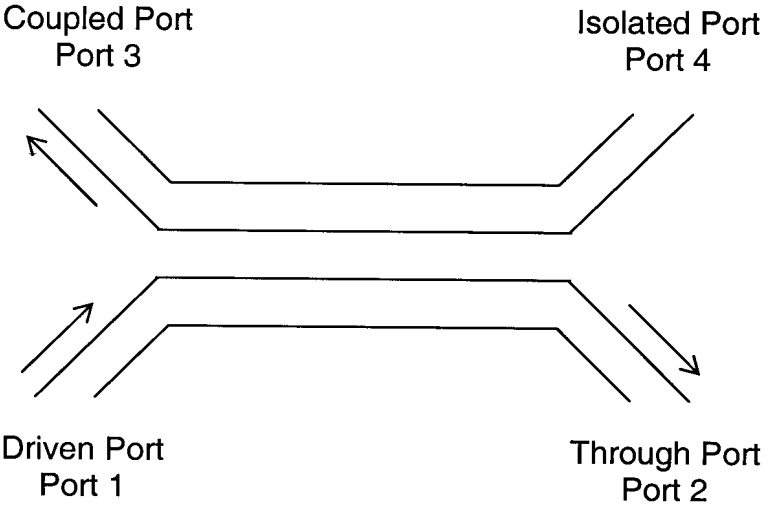

Figure 3.1. The Coupled-Line Directional Coupler.

The equivalent circuit for the directional coupler is shown in Figure 3.2. The even-mode and odd-mode impedances refer to the entire two-line structure.

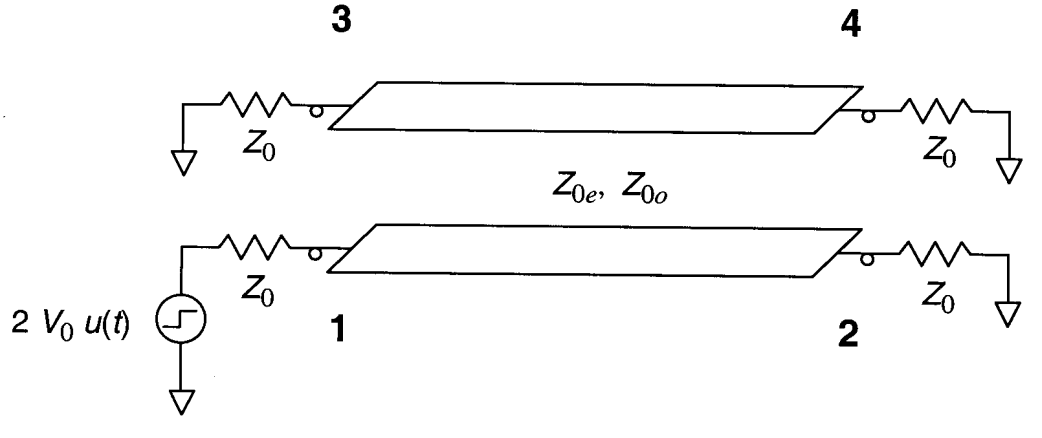

Figure 3.2. Equivalent circuit of the directional coupler.

Next, we decompose the equivalent circuit into even and odd modes, as shown in Figure 3.3. By adding the results from the two modes, one obtains the result for the directional coupler when driven as shown in Figure 3.2.

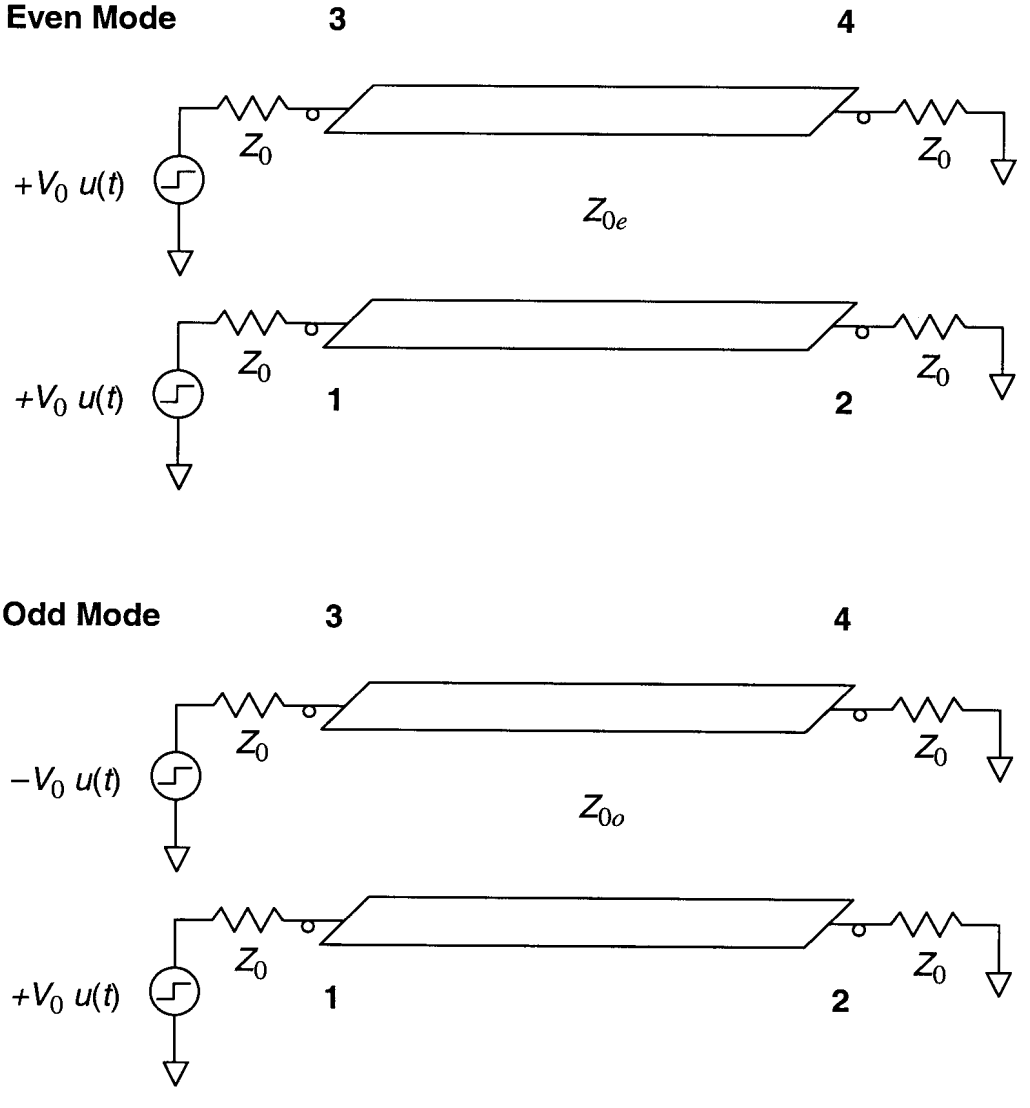

Figure 3.3. Decomposition of the directional coupler into even and odd modes.

Finally, we separate the even and odd modes each into a single transmission line, which is allowable because of the symmetry of the modes. The result is shown in Figure 3.4. Note that when separating the two lines, one has to double the even mode impedance and halve the odd-mode impedance. Note also that the sign of the voltage generator in the odd mode has to be chosen to conform with either the top or bottom transmission line in Figure 3.3.

Even Mode (Single Line)

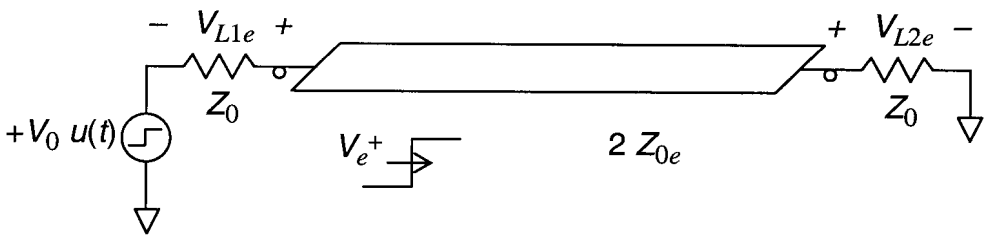

Odd Mode (Single Line)

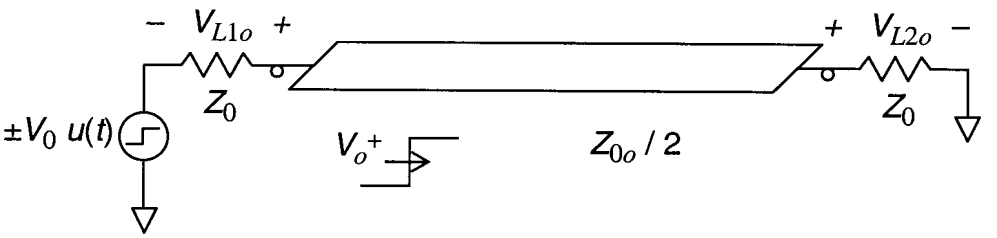

Figure 3.4. The single-line representations of the even and odd modes of the directional coupler.

Port 3: Coupled Port

At Port 3, the voltage is the sum of the voltages across the first load resistor for the even- and odd-mode cases. For the even mode, the voltage across the near load resistor is calculated by voltage division in Figure 3.4 as

$$V_{L1e} = -V_0 \frac{Z_0}{Z_0 + 2Z_{0e}} \tag{3.1}$$

where we have dropped the step-function time dependence, $u(t)$. The above expression is valid for one round-trip transit time of the transmission line. Similarly, the voltage across the near load in the odd mode is

$$V_{L1o} = V_0 \frac{Z_0}{Z_0 + Z_{0o}/2} \tag{3.2}$$

Note that we have used the minus sign in the odd-mode source, because we are calculating a port on the top transmission line. The total voltage at port 3 is the sum of the even-mode and odd-mode results, or

$$V_3 = V_{L1e} + V_{L1o} \tag{3.3}$$

Combining the above three equations we have

$$V_3 = -V_0\left(\frac{Z_0}{Z_0 + 2Z_{0e}} - \frac{Z_0}{Z_0 + Z_{0o}/2}\right) \tag{3.4}$$

To simplify the above expression, we hypothesize that the correct relationship between the odd-mode and even-mode impedance is

$$Z_0 = \sqrt{Z_{0e}\, Z_{0o}} \tag{3.5}$$

This hypothesis is based on the well-known frequency-domain solution to this problem, such as that in [2]. Later in this section, we show that if equation (3.5) is satisfied, the voltage into the isolated port, Port 4, is zero. This is the condition required to describe a device as a directional coupler.

If we now combine the above two equations and simplify, we obtain

$$\boxed{V_3 = V_0\left(\frac{2Z_{0e} - Z_0}{2Z_{0e} + Z_0}\right)} \tag{3.6}$$

This is the voltage into Port 3, the coupled port, for one round-trip transit time of the coupled line.

Port 1: Driven Port

Next, we calculate the voltage across the source resistor, which is the same as the voltage seen by Port 1. To do so, we note that this problem is almost identical to the calculation of the Port 3 voltage. The only change necessary is to change the sign of the odd-mode voltage source in equation (3.2). After adding the even-mode and odd-mode contributions, and after imposing equation (3.5), we find.

$$\boxed{V_1 = V_0} \tag{3.7}$$

Once again we have dropped the step-function time dependence, and this is valid only for one round-trip transit time of the transmission line. This result is somewhat reassuring, because if the source were driving a 50-ohm load instead of a directional coupler, we would get the same result.

Port 2: Through Port

Next, we calculate the voltage that gets through the directional coupler, and is deposited into Port 3. To begin this calculation, we calculate the voltage wave launched onto both the even-mode and odd-mode transmission lines, as

$$\begin{aligned} V_e^+ &= V_0\left(\frac{2Z_{0e}}{Z_0+2Z_{0e}}\right) \\ V_o^+ &= V_0\left(\frac{Z_{0o}/2}{Z_0+Z_{0o}/2}\right) \end{aligned} \tag{3.8}$$

Note that we have used the positive sign on the odd-mode voltage source. The voltage deposited onto the resistor at the far end of the transmission line is calculated by the standard transmission coefficient, $2Z_2/(Z_1+Z_2)$, so

$$\begin{aligned} V_{L2e} &= V_e^+\left[\frac{2Z_0}{(Z_0+2Z_{0e})}\right] = V_0\left[\frac{4Z_0Z_{0e}}{(Z_0+2Z_{0e})^2}\right] \\ V_{L2o} &= V_o^+\left[\frac{2Z_0}{(Z_0+Z_{0o}/2)}\right] = V_0\left[\frac{Z_0Z_{0o}}{(Z_0+Z_{0o}/2)^2}\right] \end{aligned} \tag{3.9}$$

By incorporating the geometric mean condition, equation (3.5), we find

$$V_{L2e} = V_{L2o} = V_0\left[\frac{4Z_0Z_{0e}}{(Z_0+2Z_{0e})^2}\right] \tag{3.10}$$

Now the voltage into Port 2 is simply the sum of the even-mode and odd-mode voltages, or

$$V_2 = V_{L2e} + V_{L2o} \tag{3.11}$$

So the voltage into Port 2, the through port, is

$$\boxed{V_2 = V_0\frac{8Z_0Z_{0e}}{(Z_0+2Z_{0e})^2}} \tag{3.12}$$

This voltage is valid from the time it first hits the far end of the transmission line until one round-trip transit times afterward.

Port 4: Isolated Port

Finally, we calculate the voltage into the isolated port, Port 4. This calculation is nearly identical to that of Port 2, except that the source for the odd mode now is negative. This inverts the voltage driven at the far end of the odd-mode transmission line, with the result that

$$V_{L2e} = -V_{L2o} = V_0\left[\frac{4Z_0Z_{0e}}{(Z_0+2Z_{0e})^2}\right] \tag{3.13}$$

The voltage into Port 4 is just the sum of the above two voltages, or

$$\boxed{V_4 = 0} \tag{3.14}$$

We now see that the geometric mean condition imposed in equation (3.5) leads to the crucial result necessary to have a directional coupler, i.e. $V_4 = 0$.

4. Optimal Design

Having calculated the voltages for the four ports of the coupler, we now optimize the choice of the even-mode impedance, Z_{0e}. Once this is specified, the odd-mode impedance is specified by equation (3.5).

We need to satisfy competing requirements in the directional coupler. On the one hand, we need the transmitted signal at Port 2, to be as high as possible. We define a transmission coefficient as

$$T = \frac{V_2}{V_1} = \frac{8Z_0Z_{0e}}{(Z_0+2Z_{0e})^2} \tag{4.1}$$

At the same time, we require the signal coupled into the receiver be as high as possible. Thus we define a coupling coefficient as

$$C = \frac{V_4}{V_2} = \frac{V_3}{V_1} = \frac{2Z_{0e}-Z_0}{2Z_{0e}+Z_0} \tag{4.2}$$

The optimal directional coupler is achieved when we maximize the product $C \times T$, which we define as the function η, so

$$\eta(r) = T \times C = \frac{8r(2r-1)}{(2r+1)^3}$$
$$r = \frac{Z_{0e}}{Z_0} \tag{4.3}$$

We plot $\eta(r)$ as a function of r in Figure 4.1. We see that the optimal value of $\eta(r)$ occurs at r = 1.85, where η_{opt} = 0.385. But the maximum is rather broad, so there is very little compromise in performance if one uses r = 1.5, where η = 0.375. In fact, this lower value of r is much easier to implement physically, so that is probably the preferred configuration. At this value of r, Z_{0e} = 75 Ω, and Z_{0o} = 33.3 Ω, and C = 0.5, resulting in a 6-dB directional coupler.

It is interesting to note that the above theory predicts a second optimum at r=0.133, which has the same figure of merit, $|\eta|$ = 0.385. However, this configuration leads to Z_{0e} = 6.7 Ω and Z_{0o} = 376 Ω, which we believe is not physically realizable.

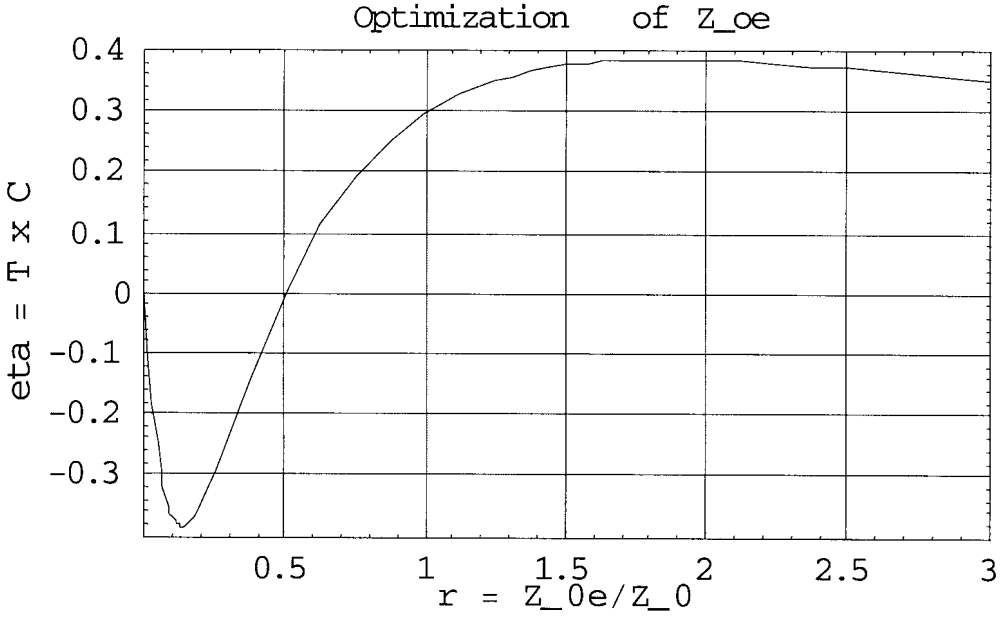

Figure 4.1. The optimization function for the symmetrical coupled-line directional coupler.

5. Directional Coupler Fabrication

We built two versions of the directional coupler based on the design criteria of the previous section combined with high-voltage considerations. We experimented with a number of different cross sections, and we finally settled on the cross section shown in Figure 5.1. This design is composed of two pieces of half-round stock parallel to each other and separated by a 25-mil film of UHMW polyethylene. We built the outer shell of the directional coupler as a round cylinder that is positioned coaxial to the coupled conductors. We chose this particular shape because it simplified our impedance calculations and because it was relatively simple to build.

The impedances were estimated as follows. The even-mode impedance was estimated with the formula for a coaxial cable, ignoring the small gap between the two piece of half-round stock. The odd-mode impedance was estimated with the formula for two parallel plates with no fringe fields. These calculations were confirmed by finite element analysis using MATLAB and the Partial Differential Equation toolbox.

The entire configuration is immersed in oil. Both oil and UHMW have a dielectric constant of about 2.3. The conductor separations (in oil and by the UHMW polyethylene) are designed to provide a high-voltage standoff better than 50 kV.

We built two versions of this coupler, an asymmetrical design, shown in Figure 5.2, and a symmetrical design, shown in Figure 5.3. Photos of the two directional couplers are shown in Figure 5.4. We built the two designs because the asymmetrical design was simpler to build, but the symmetrical design was believed to have smaller spurious effects where the two transmission lines merge.

$D = 3.2$ in
$s = 0.025$ in $\qquad d = 0.25$ in
$Z_{0e} = 100.6\ \Omega \qquad Z_{0o} = 24.9\ \Omega$
$\ell = 12$ inches $\qquad C = 0.6$, or -4.4 dB
$\varepsilon_r = 2.3$ dielectric constant (oil and UHMW)
dielectric strength = 2000 V/mil (UHMW)
dielectric strength = 250 V/mil (transformer oil)

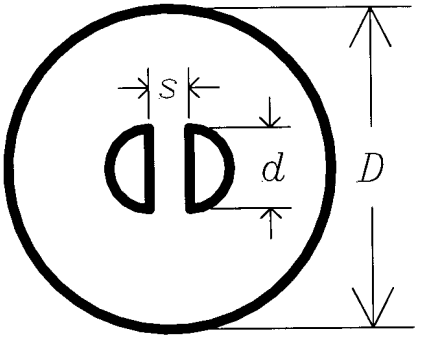

Figure 5.1. Cross section of the coupled-line directional coupler.

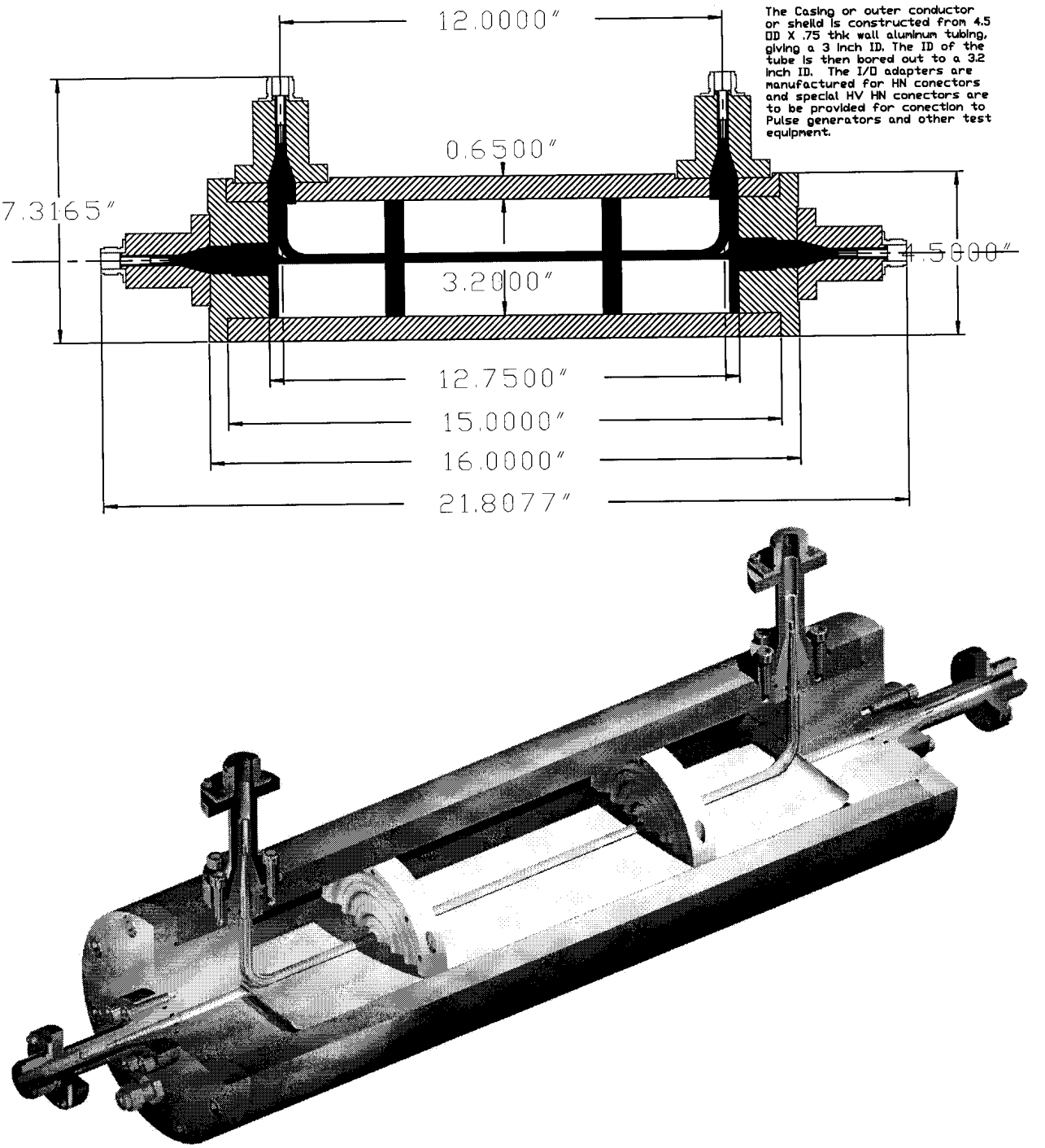

Figure 5.2. The asymmetrical design of the coupled-line directional coupler.

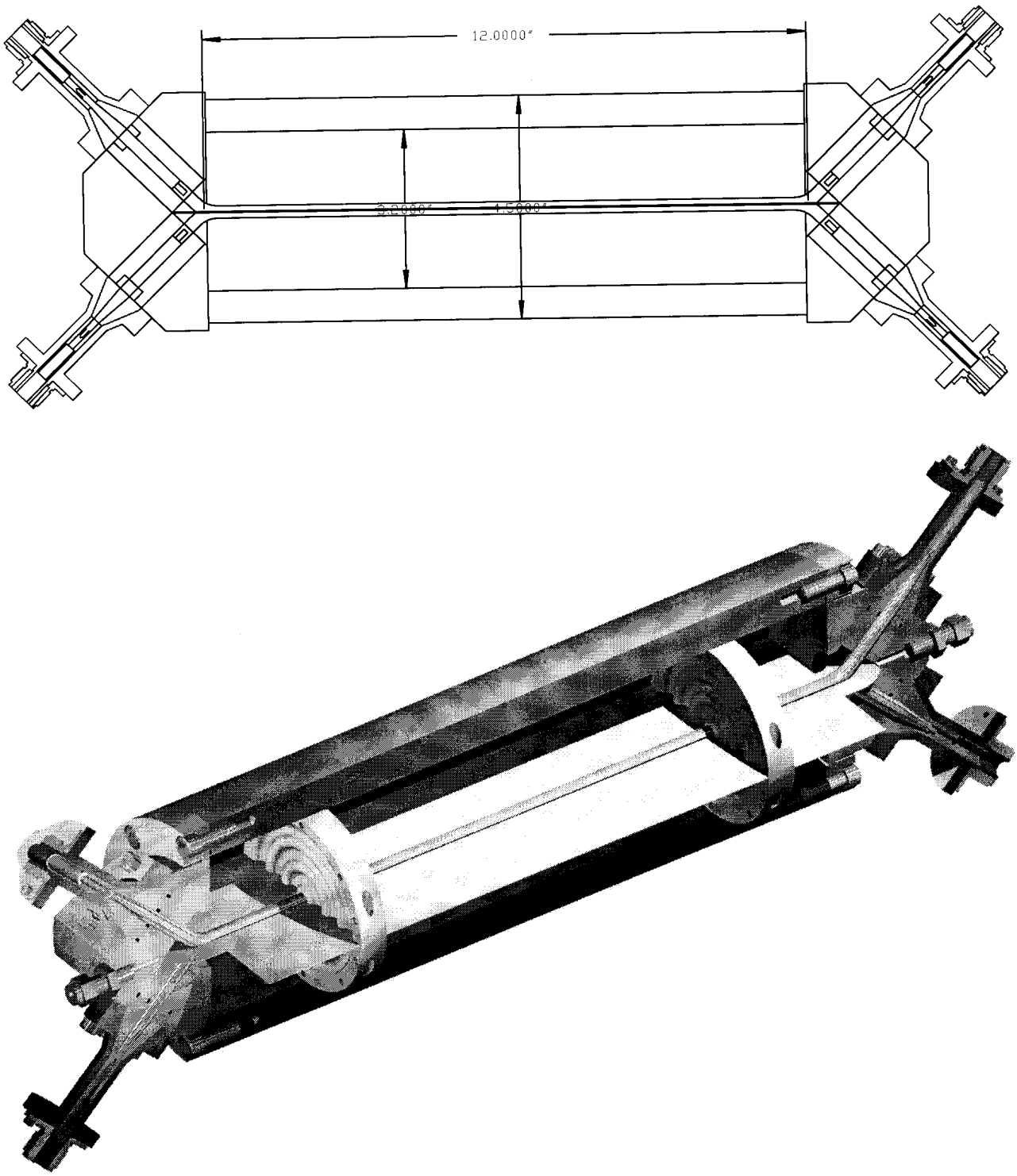

Figure 5.3. The symmetrical design of the coupled-line directional coupler.

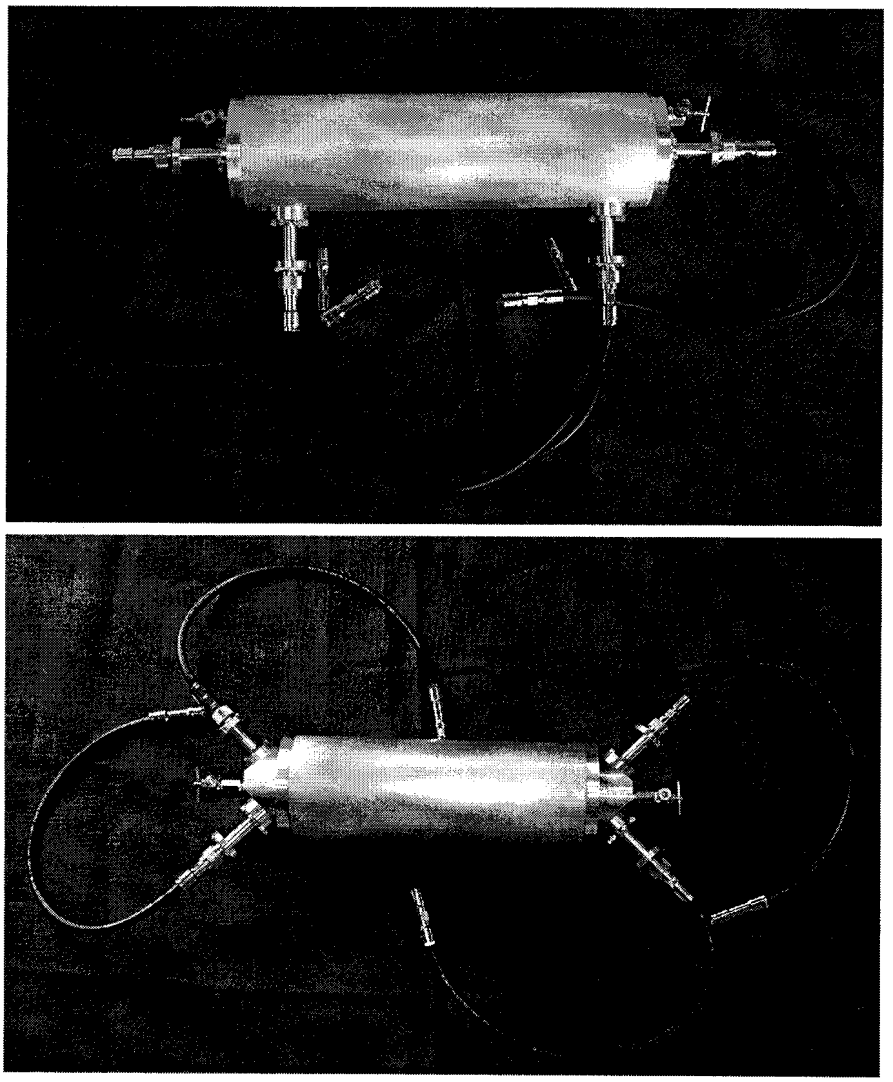

Figure 5.4. Photos of the asymmetrical (top) and symmetrical (bottom) directional couplers.

The directional couplers are equipped with modified HN-Type connectors at each port. Equal-length RG213 cables provide transition from the modified HN-Type connectors to standard HN connectors, and ultimately to HN-to-SMA adaptors for the low-voltage testing.

6. Directional Coupler Testing

6.1. Impedance Measurements

We began our measurements with a variety of TDR measurements using the Tektronix model TDS8000 sampling scope and the 80E04 sampling module. We measured both single-channel and differential-mode impedances. We measured the single-channel impedance to determine the 50-ohm match of the properly terminated coupler, and the differential-mode impedances to determine the odd- and even-mode impedances on the coupled line. This data allows us to diagnose possible impedance discontinuities in the device.

We plot the TDR of the both couplers in Figures 6.1 and 6.2, for both Port 1 and Port 3. In theory, these TDRs should be a flat 50 ohms out to late times, since the other three ports are terminated in 50 ohms. Therefore, these TDRs can be used to determine how accurately the couplers have been built and to isolate areas of impedance discontinuity. Our TDRs are centered on 50 ohms, but they vary over a range of 32 to 73 ohms at early time. The locations and magnitudes of the impedance discontinuities can be used as a diagnostic to improve the smoothness of the response of future couplers.

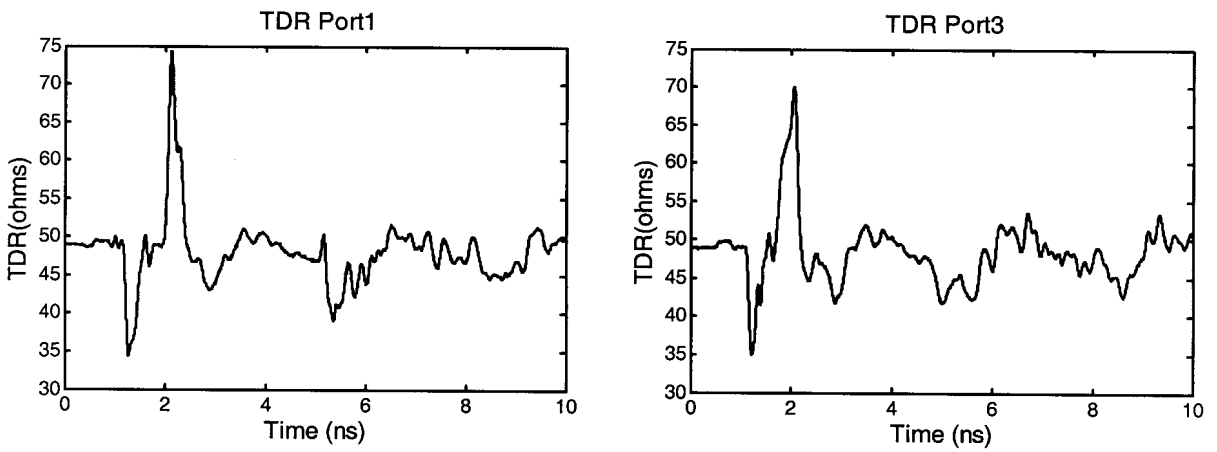

Figure 6.1. TDRs of the asymmetrical directional coupler for Port 1 (left) and Port 3 (right).

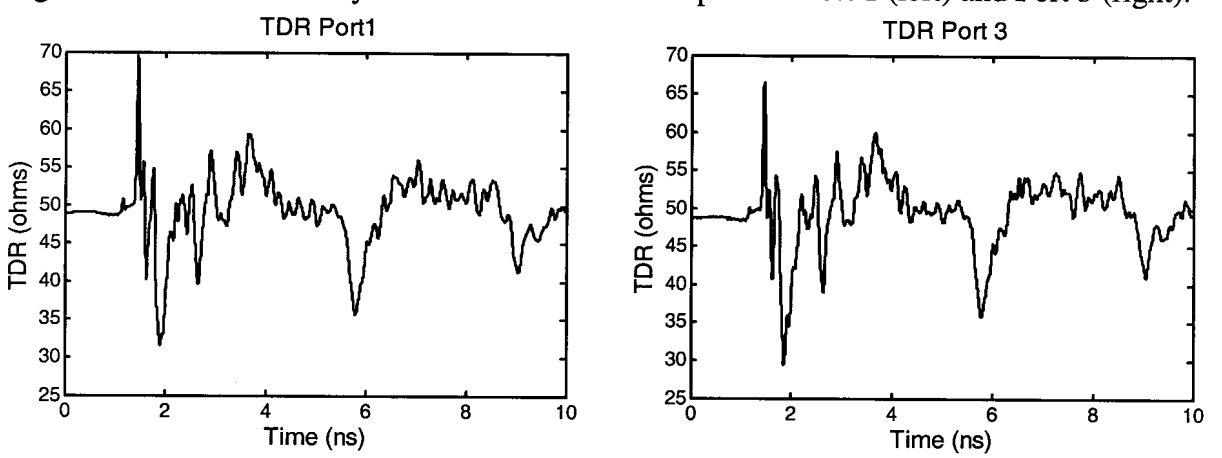

Figure 6.2. TDRs of the symmetrical directional coupler for Port 1 (left) and Port 3 (right).

We also measured the even-mode and odd-mode impedance of the coupler. We did this by driving Ports 1 and 3 with identical pulses with either the same or opposite polarity. The results are shown in Figure 6.3 for the even mode on the left, and for the odd mode on the right. The even-mode and odd-mode impedances should be about 100 ohms and 25 ohms, respectively, to match our design criteria. We observe impedances of about 90 ohms and 23 ohms, so we are in reasonable agreement with our predictions.

Similarly we measured the differential impedances of the symmetrical coupler. The results are shown in Figure 6.4 for the even mode on the left, and for the odd mode on the right. Again, the even-mode and odd-mode impedances should be about 100 ohms and 25 ohms, respectively. We observe impedance of about 95 ohms and 25 ohms, so we are again in reasonable agreement with our predictions.

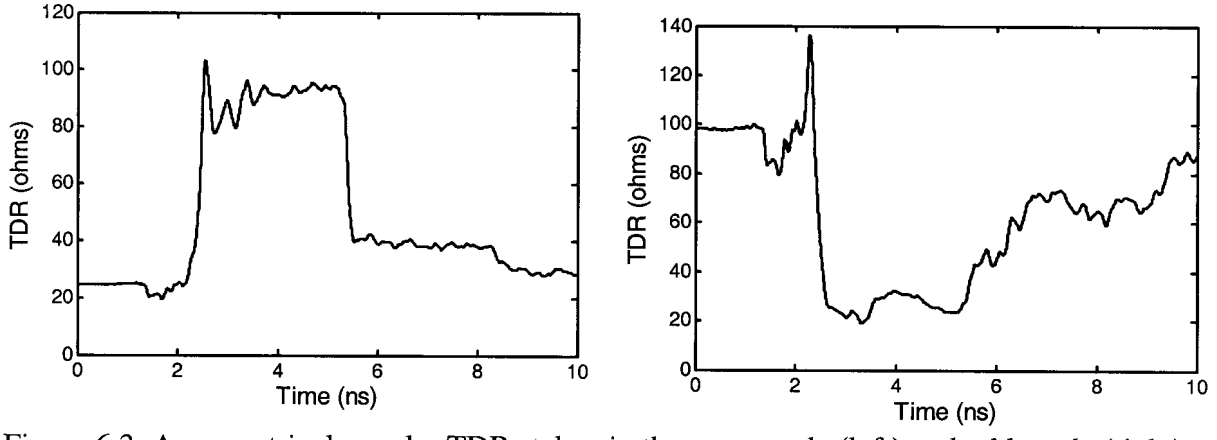

Figure 6.3. Asymmetrical coupler TDRs taken in the even mode (left) and odd mode (right).

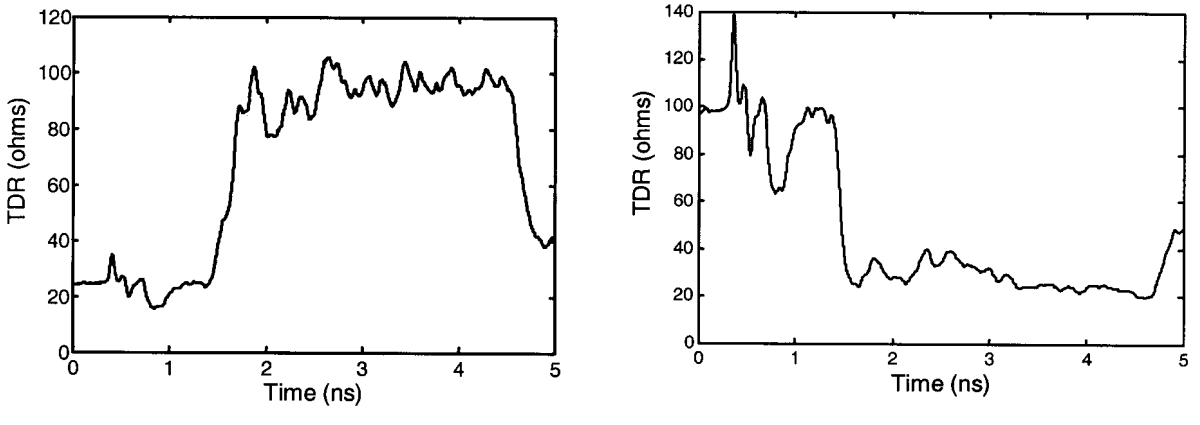

Figure 6.4. Symmetrical coupler TDRs taken in the even mode (left) and odd mode (right).

6.2. Time Domain Outputs of the Directional Couplers

We used a Kentech model ASG1 pulse generator to drive the directional coupler at the driven port, Port 1. The ASG1 has a peak voltage of 230 V, a risetime of 100 ps, and a long exponential decay, as seen in Figure 6.5. We recorded the outputs at each of the three non-driven ports. Our goal for this measurement is to determine the ratio of the peak outputs of the three outputs compared to the driving pulse, and compare those ratios to the predicted values.

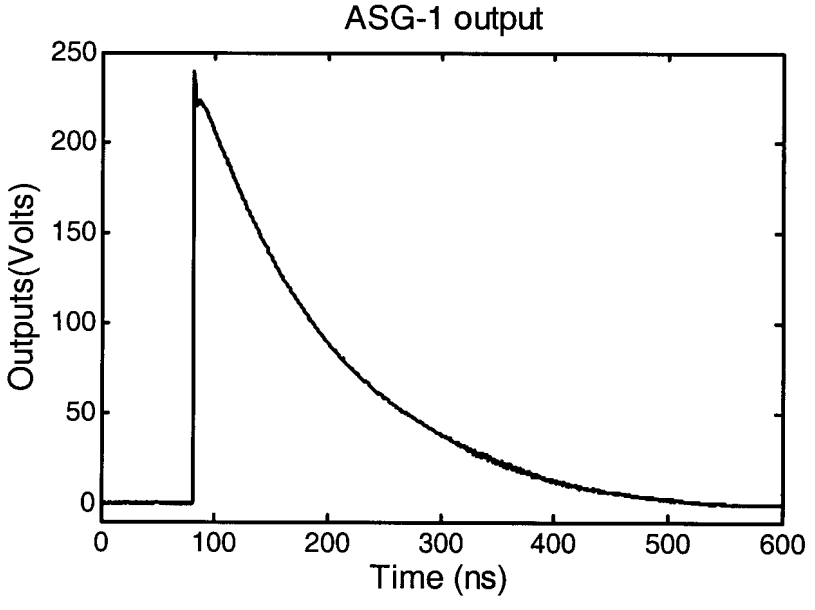

Figure 6.5. ASG1 output.

Asymmetrical Coupler

We begin with our measurements of the asymmetrical directional coupler. The raw waveforms are shown in Figure 6.6, where we see that all the waveforms are nearly flat for one round-trip transit time. The voltages at the coupled and through ports have nearly the same initial values. A summary of the initial values relative to the peak input voltage of 230 volts is provided in Table 6.1. These values are compared to the theoretical values as determined from section 3. While the initial waveforms are approximately flat for the first 3 ns, we observe that there is actually some variation in the waveforms. Thus, the initial values of the waveforms are subject to some interpretation, and we have tried to record the average values in the table. The agreement between theoretical and experimental values is not too bad, but the measured value at the through port is 1.9 dB lower that we expected. We also observe an increase in risetime, and possibly some effects due to the connectors. The output at the isolated port is approximately 20 dB down from the source.

In Figure 6.6 we also plot the transmission data on a longer time scale, to show the reflections occurring at late times. The coupler is twelve inches long in oil, which corresponds to a round-trip transit time of 3 nanoseconds. One can deconvolve the reflections in order to obtain a clean impulse response.

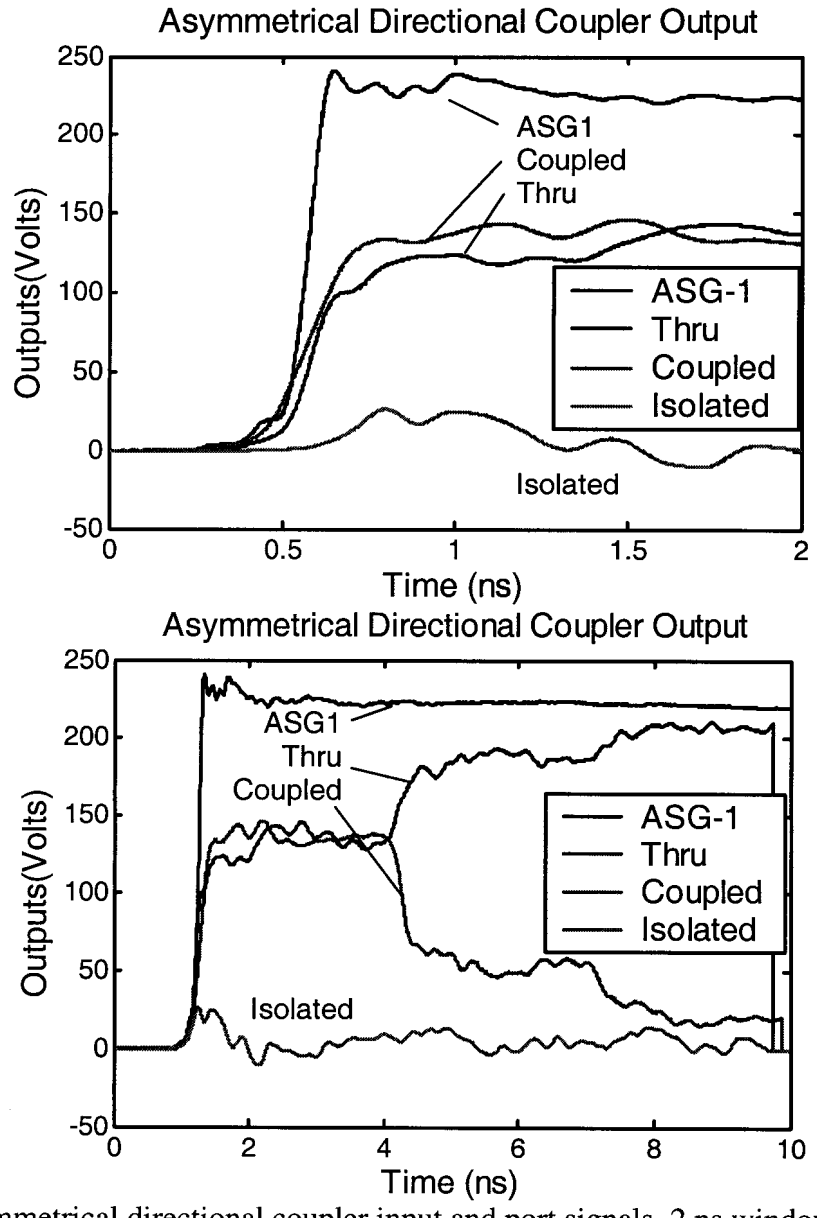

Figure 6.6. Asymmetrical directional coupler input and port signals, 2 ns window (top) and 10 ns window (bottom).

Table 6.1. Summary of Results for the Asymmetrical Directional Coupler

Port	**Measured Relative Initial Value**	**Theoretical Relative Initial Value**
Coupled	0.56 (–5.0 dB)	0.60 (-4.4 dB)
Through	0.52 (–5.7 dB)	0.64 (–3.8 dB)
Isolated	0.1 (–20 dB)	0.00 (– ∞ dB)

Symmetrical Coupler

We built the symmetrical version of the coupler because it had more promise for providing a smoother response at the transition points. However, this is a more complex design to build because of the 45-degree angles, so it is more challenging to maintain the tight tolerances that are required for this design. For this measurement we added a 100 pF blocking capacitor to the output of the ASG1 to shorten its fall time to around 6 ns.

We now present the port waveform measurements of the symmetrical directional coupler. The raw waveforms are shown in Figure 6.7, where Port 1 is the input port, Port 2 is the through port, Port 3 is the coupled port and Port 4 is the isolated port. We see that the coupled and through ports have nearly the same initial values. A summary of the initial values relative to a peak input voltage of 220 volts is provided in Table 6.2. These values are compared to the theoretical values as determined from Section 3 of this report. We expect the initial waveforms to be flat for the first 3 ns, but there is actually some structure. Therefore the initial values of the waveforms are subject to some interpretation, and we have recorded the initial peak values in the table. The agreement between theoretical and experimental values is not bad, but the through port is 1.5 dB lower than we expected. We also observe a slower risetime from the through port than the input pulse. The isolated port is approximately 20 dB down from the source. Overall the symmetrical coupler data is slightly better than that of the asymmetrical coupler.

6.3. Discussion of the Directional Coupler Results

We found that both directional coupler designs generally performed as expected. In both cases, we observed a relative initial value for the through port that was somewhat lower than the theory predicts. For the asymmetrical case the measurement was low by 1.9 dB, and for the symmetrical case the measurement was low by 1.5 dB. But this can be explained by the very small separation between the two lines (25 mils). By maintaining a very close separation between the two lines, losses due to finite conductivity are increased. In future designs, we can increase the separation, because of the calculations in Section 4 showing how to optimize the choice of impedance. These results show that an even-mode impedance as low as 75 ohms is reasonable, instead of the 100-ohm even-mode impedance used here. The lower impedance allows a larger separation between the two lines, which results in lower losses.

To refine the design, we will smooth those points in the structure that correspond to the rough spots in the TDR. We will also use a larger separation between the parallel lines, to reduce the transmission losses. Finally, we will use a longer coupler with a longer clear time. Our working assumption is that the bandwidth of the coupler is equal to the inverse of the round-trip transit time. For example, our 30-cm-long coupler has a round-trip transit time of 3 ns in oil, so it should reach as low as 333 MHz. By this calculation, to reach as low as 100 MHz requires a coupler one meter long. We should test this hypothesis, to see if we have the correct relationship between frequency range and transit time. A shorter coupler will have a lower transmission loss, so there is some incentive to keep it as short as possible.

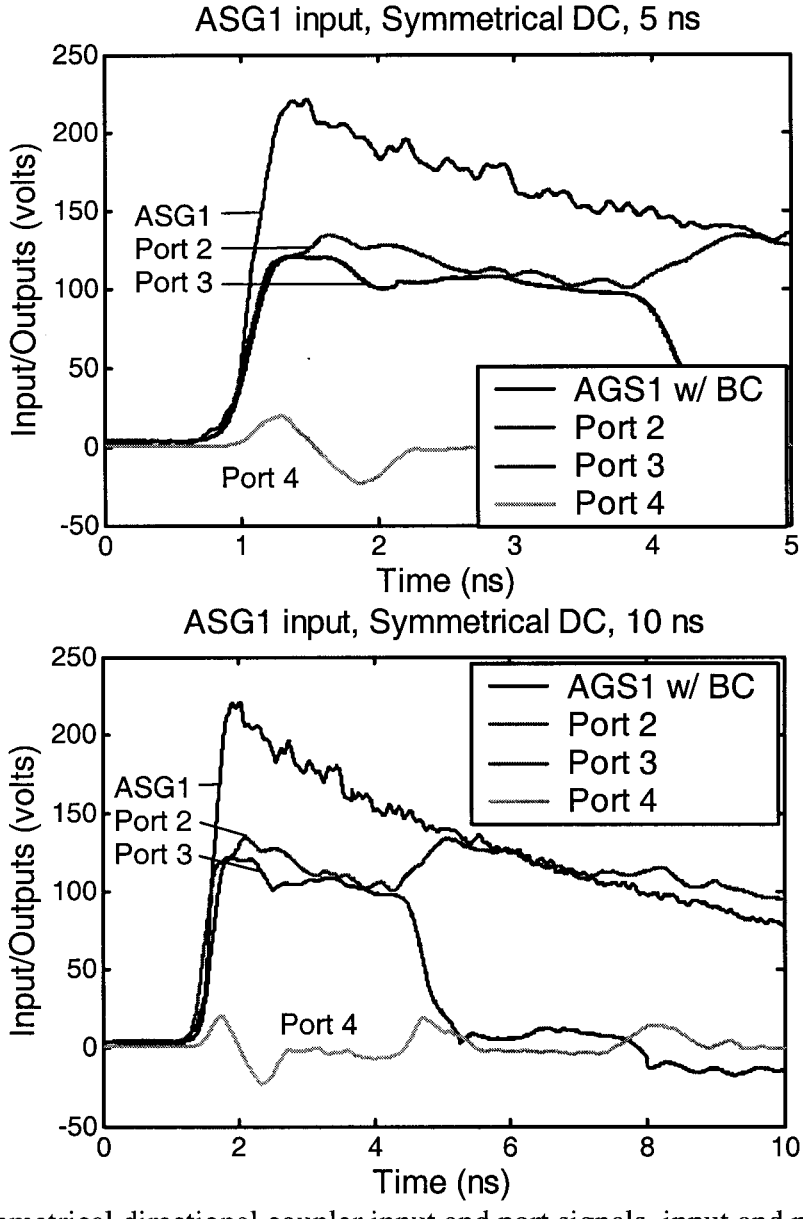

Figure 6.7. Symmetrical directional coupler input and port signals, input and port signals, 5 ns window (top) and 10 ns window (bottom).

Table 6.2. Summary of Results for the Symmetrical Directional Coupler

Port	Measured Relative Initial Value	Theoretical Relative Initial Value
Coupled	0.55 (–5.3 dB)	0.60 (-4.4 dB)
Through	0.55 (–5.3 dB)	0.64 (–3.8 dB)
Isolated	0.1 (-20 dB)	0.00 (– ∞ dB)

7. Radar Measurements

To test the directional couplers, we created a prototype impulse radar system as shown in Figure 7.1. We drove the IRA with a 4-volt Picosecond Pulse Labs 4015C that was fed through the directional coupler. The target, a 60-centimeter triangular trihedral corner reflector, is shown in Figure 7.2. A photo of the UWB transceiver is shown in Figure 7.3. Our transceiving antenna was a Farr Research impulse radiating antenna, model IRA-3M, shown in Figure 7.4. We received the signal on Port 4 of the directional coupler using a Tektronix TDS8000 sampling oscilloscope.

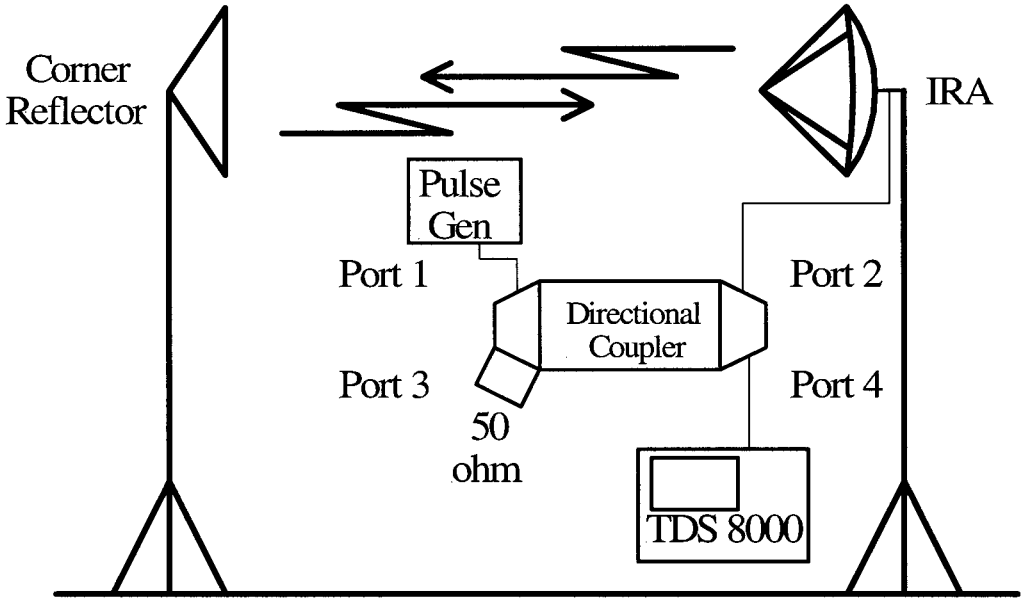

Figure 7.1. Radar test setup.

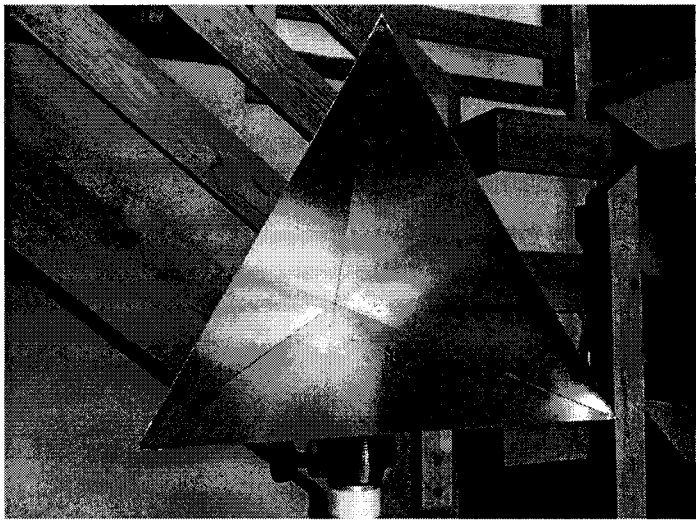

Figure 7.2. Trihedral corner reflector with 60-centimeter sides.

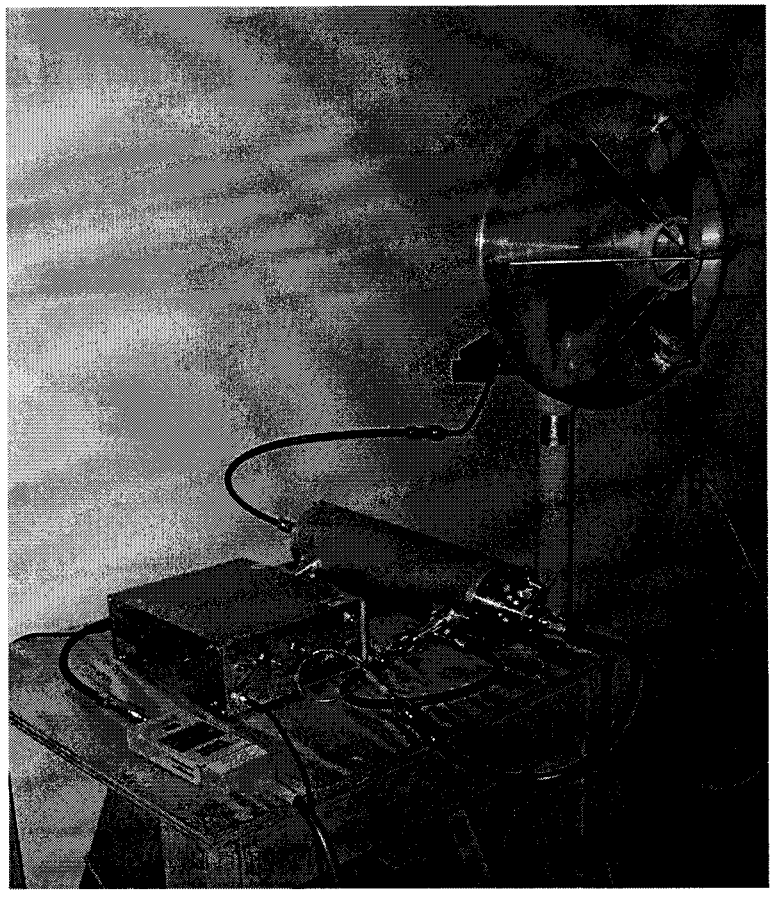

Figure 7.3. UWB Transceiver, showing from left to right, the sampling head, pulser, asymmetrical directional coupler, and antenna. The oscilloscope is not shown.

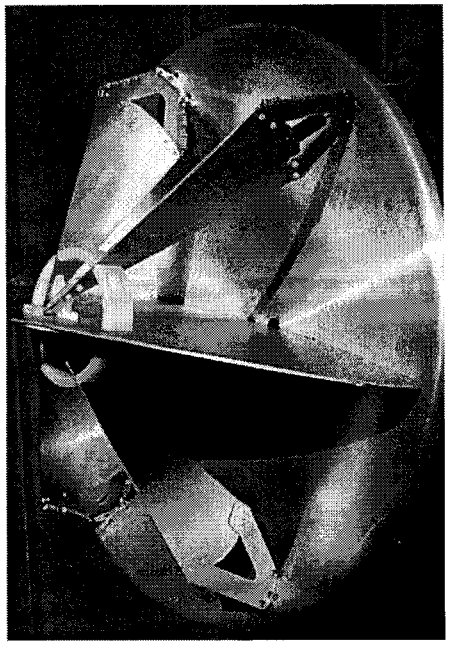

Figure 7.4. The Farr Research Model IRA-3M.

7.1. Radar Measurements with the Asymmetrical Coupler

We began our radar measurements with the asymmetrical coupler. We varied the spacing between the transceiving IRA and the corner reflector from 0 to 2.5 meters in half-meter increments. First, we measured the background clutter by recording the signal with no corner reflector present. This waveform, shown in Figure 7.5, was then subtracted from our subsequent data to remove background clutter.

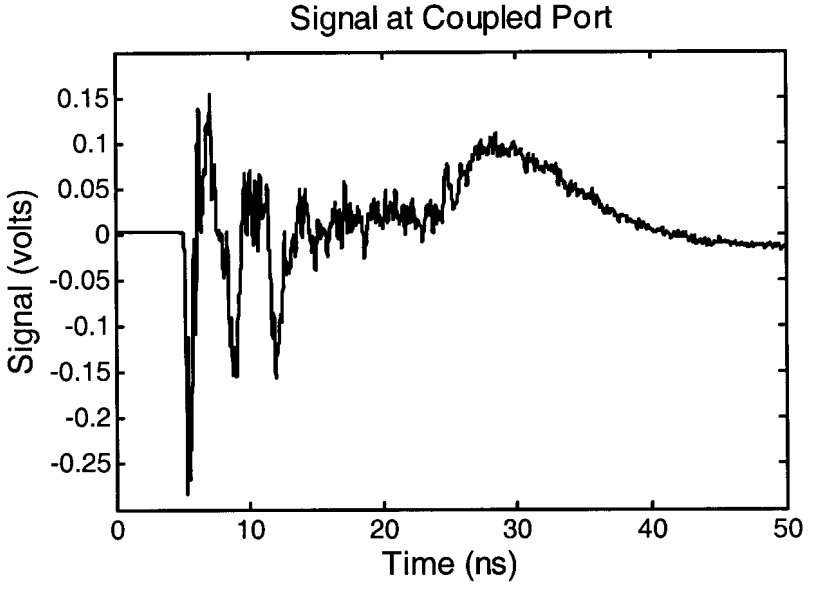

Figure 7.5. Background clutter measurement without corner reflector, used for background subtraction.

Next, we measured the returned signal from the corner reflector at a number of distances from the IRA. Starting at a distance of 0 meters from IRA (measured from the focus to the edge of the corner reflector), we moved the corner reflector away from the IRA in half-meter increments out to a distance of 2.5 meters. At each location we recorded the signal received at Port 4. Before background subtraction, the raw waveforms for all six measurements looked essentially like Figure 7.5. After background subtraction, the results reveal the radar signatures shown in Figure 7.6. In the data we see that as the corner reflector is moved away from the antenna by each half-meter increment, the backscattered signal is delayed by an additional 3.3 ns, as we expect, showing that the signal is a true reflection and not a spurious artifact.

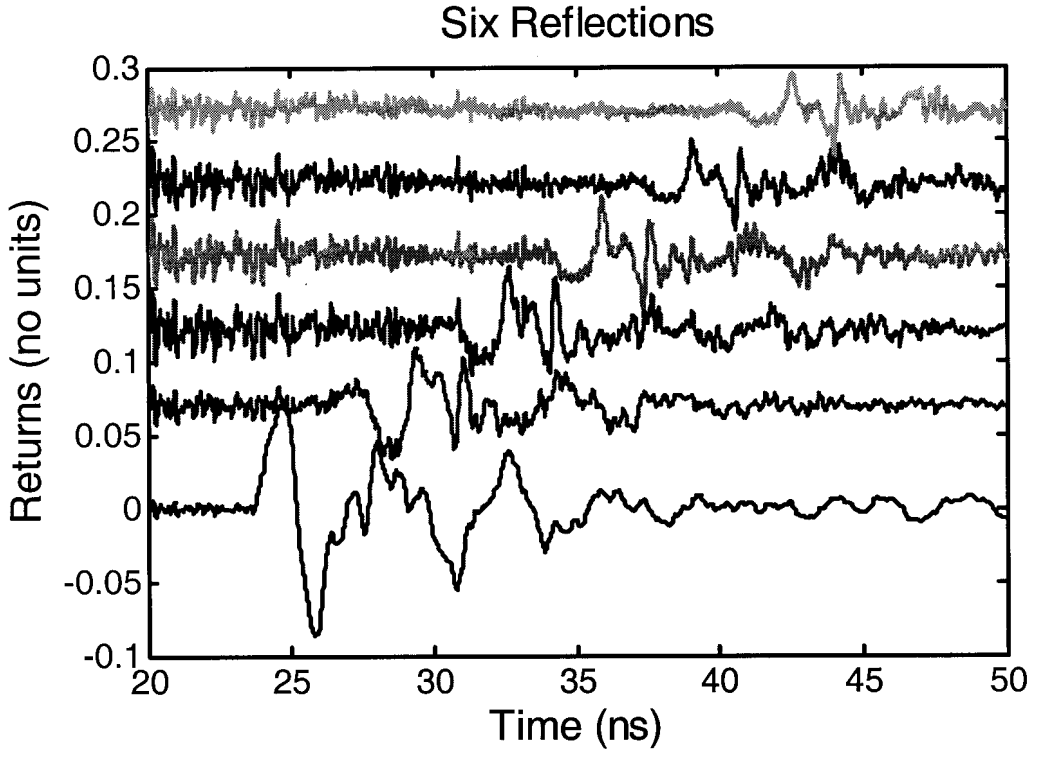

Figure 7.6. Six returns from the corner reflector, ranging in distance from 0 to 2.5 meters.

7.2. Radar Measurements with the Symmetrical Coupler

Next, we tested the symmetrical directional couple in the radar setup shown in Figure 7.1. We varied the spacing between the transceiving IRA and the corner reflector from 1 meter to 8 meters in 1-meter steps.

In Figure 7.7 we show an overlay of the signal at Port 4 with no corner reflector present, along with the eight raw return signals from the corner reflector at different locations. On this scale all nine traces are virtually indistinguishable. The coupled port signal is again the baseline for background subtraction. This signal is the superposition of the leakage signal at the isolated port and the coupled portion of the return signal. The return signal is the signal reflected back from any possible room reflections. The leakage signal is always present, and since it is much larger than the coupled return, it masks the return data. Some unchanging room reflections (ground clutter) are also present, but they will be subtracted from the data.

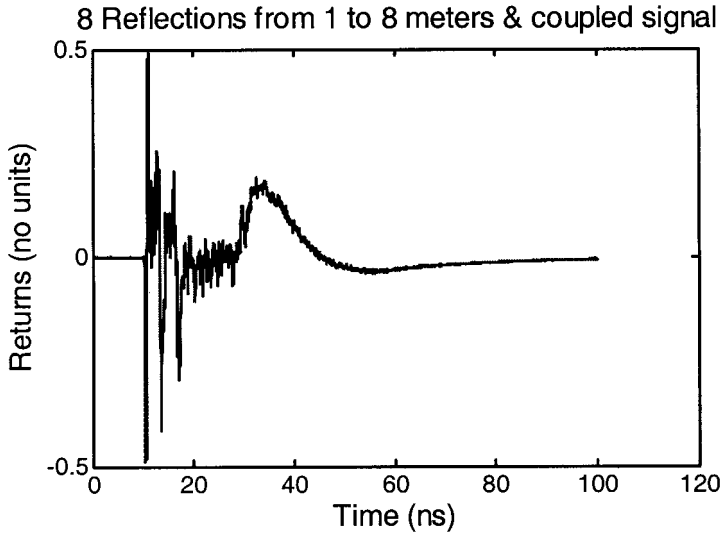

Figure 7.7. Eight corner-reflector measurements and baseline, PSPL 4015C.

To recover the scattered signal, we subtract the background signal, and the result is shown in Figure 7.8. In this figure we can identify reflections from the corner reflector as the reflection moves across the Figure in 6.6-ns increments, starting with the bottom trace and proceeding to the top. We have arbitrarily scaled the processed return data to make it roughly uniform, and we have offset the signals for clarity.

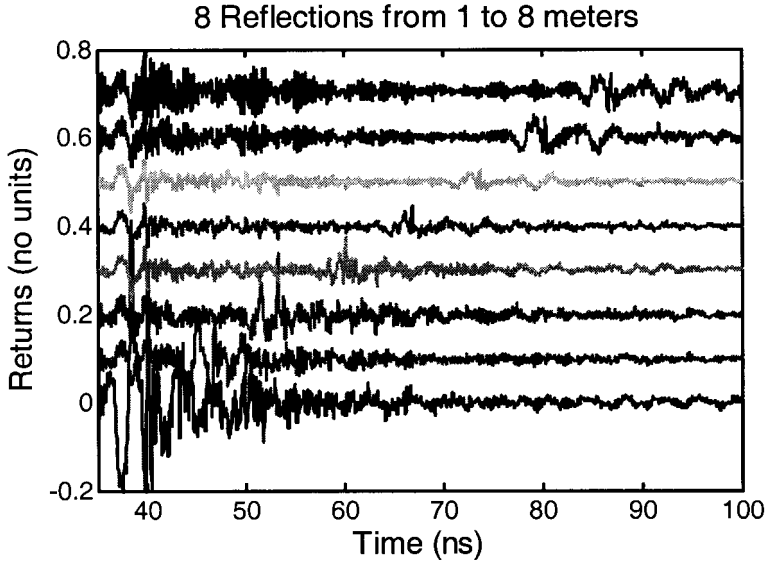

Figure 7.8. Eight returns from the corner reflector.

The bottom trace in Figure 7.8 shows the data at one-meter separation between the transceiving antenna and the reflector. The top trace shows the data at 8 meters separation. In the figure we see corner-reflector return marching out in time in 6.6 ns increments, corresponding to 1-meter increments in separation, as we proceed from bottom to top. Additional filtering of the return signals, shown in Figure 7.9, reduces the noise, showing the return data more clearly.

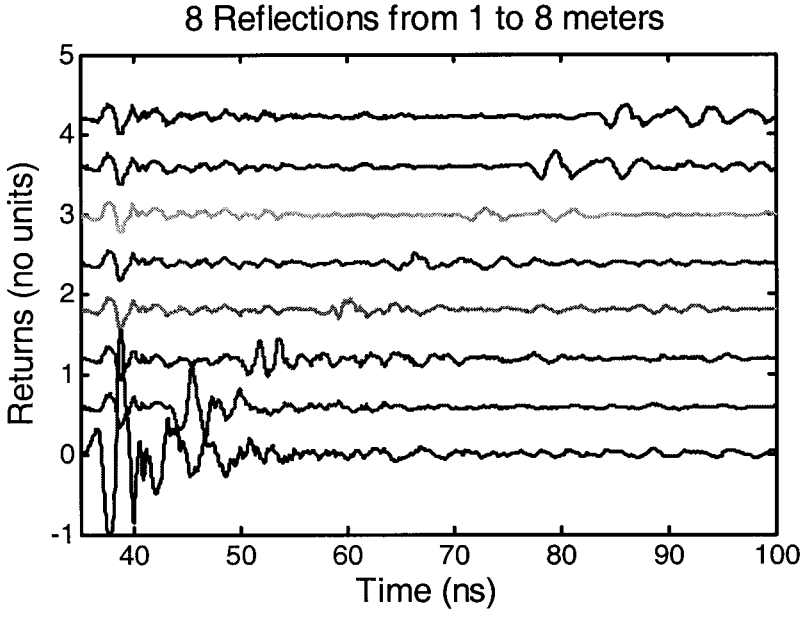

Figure 7.9. Eight reflections from the corner reflector, with filtering.

We conclude that we are obtaining very promising data from both directional couplers using a corner reflector with a small antenna (18-inch diameter) and a small pulser (4-volts) with fast risetime (20 ps).

7.3. Pulse Generator Selection

We used two pulse generators during our radar testing: a Picosecond Pulse Laboratory (PSPL) model 4015C, and a Kentech model ASG1. The PSPL 4015C has a 4-volt, 20 ps risetime output, as shown in Figure 7.10. The 4015C has a fall time on the order of 10 ns. The ASG1 has a 230-volt, 180-picosecond risetime output, as shown is Figure 7.12. The ASG1 has a 10% decay time of around 300 ns.

In our radar setup of the previous section, we replaced the 4015C with the ASG1, to see if we could increase the voltage and range of the radar system. However, with the ASG1 we were never able to resolve the radar returns. We suspected the problem was that the ASG1 has too long a waveform. This waveform has a 1/*e* decay time of around 120 ns and a 10% decay time of 300 ns. This large, broad pulse saturates the oscilloscope protection limiter while receiving the reflections from the scatterer, so the limiter clips the scattered data. The limiter we used was an HP 11867A, with a frequency range to 1.8 GHz.

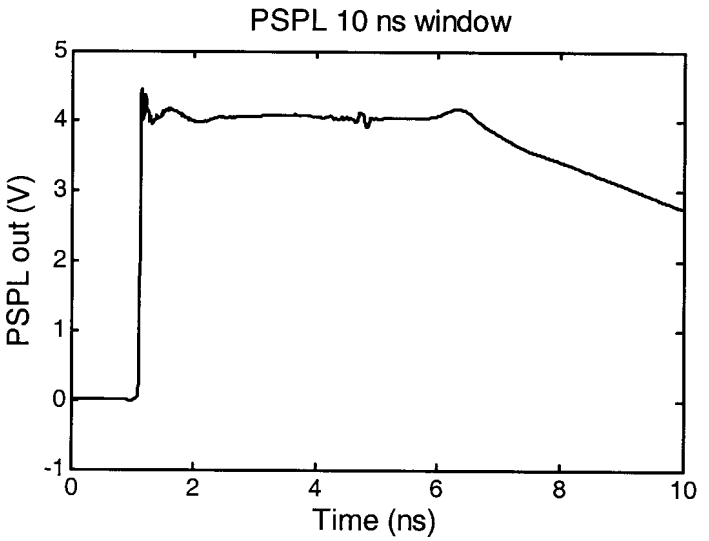

Figure 7.10. Output of the Picosecond Pulse Laboratory model 4015C pulse generator.

We tried two methods to get the ASG1 pulser to work in our radar system. First we eliminated the limiter entirely, so that it could not be saturated. This made it necessary to attenuate further the oscilloscope input to avoid overdriving the scope. The result was that we could not extract the radar return from the large ambient signal.

In a second attempt to use the ASG1, we took its derivative before using it in the radar system. To do so, we built an impulse-forming network (IFN) with a blocking capacitor. The IFN was built from two SMA panel-mount receptacles, one jack and one plug, placed end to end. We machined down the center-conductors on each connector so they were flush with the dielectric. This left two center conductors that, looking end-on, were solid disks 1.3 mm in diameter. When the two connectors were placed together, each disk acted as one plate of a round, parallel-plate capacitor. The two (center-conductor) plates of the capacitor were separated by a circular dielectric sheet. A copper-tape gasket between the two mounting plates prevented the screw tension from crushing the dielectric sheet and shorting the two center conductors. Figure 7.11 shows the completed blocking capacitor.

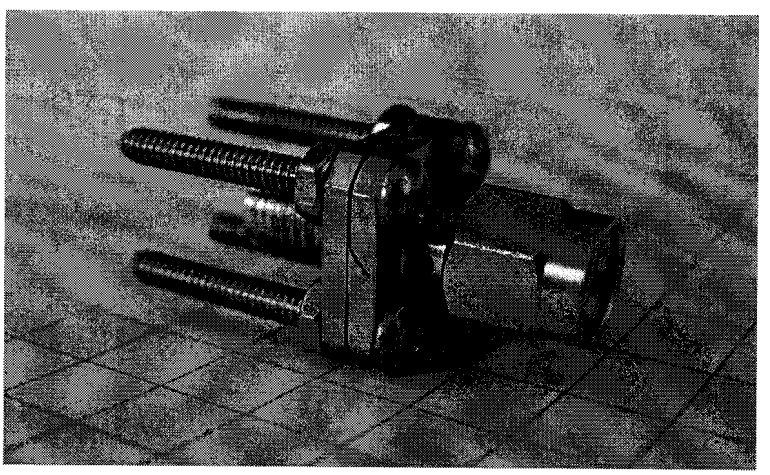
Figure 7.11. Blocking Capacitor.

The capacitance value can be estimated with the formula:

$$C = \varepsilon \frac{A}{d} \tag{7.1}$$

where

ε_r	=	relative dielectric constant of the separating sheet (~ 3)
ε_o	=	dielectric constant of free space (8.854×10^{-12} F/m)
A	=	area between the plates (~1.3×10^{-6} m^2)
d	=	distance between the plates (~7×10^{-5} m)

Using this formula, we find the capacitance for this device is about 0.5 pF.

If we combine the 0.5-pF capacitor with the 50-ohm impedance of the transmission line, we obtain a high-pass filter with an *RC* time constant, τ, of 25 ps. Recognizing that the 3-dB frequency of the differentiator is $\omega_{3dB} = 1/\tau$, we calculate a 3-dB frequency of about 6.4 GHz. Thus, this filter can be represented by a Bode plot of a first-order high-pass filter with a 3-dB frequency of 6.4 GHz. Below this frequency, the device acts as a differentiator, or an impulse forming network (IFN). The risetime of the ASG1 is about 180 ps, corresponding to a 3-dB frequency of about 1.9 GHz. So the device acts as a differentiator over a bandwidth that reaches over three times as high as the 3-dB frequency of the source.

Next, we measured the output of the combination of the Kentech model ASG1 pulser and the blocking capacitor. In figure 7.12 we show the output of the ASG1 alone, overlaid with the output of the blocking capacitor. The waveform with the blocking capacitor has been multiplied by 4.9 so the two waveforms can be easily compared. The FWHM of the capacitor output is approximately 150 ps, which is fairly close to the 180-ps measured risetime of the ASG1.

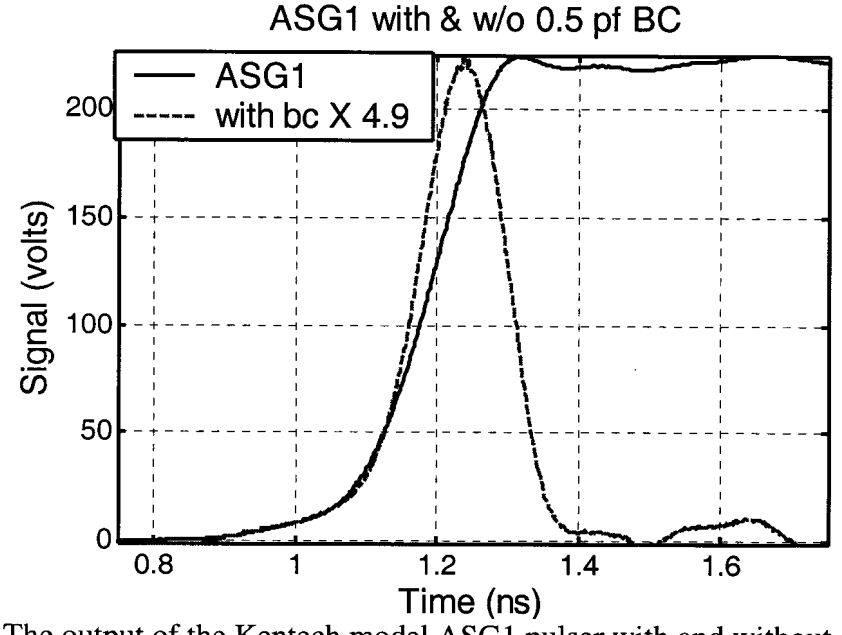

Figure 7.12. The output of the Kentech model ASG1 pulser with and without differentiator.

Finally, we incorporated the impulse forming network and ASG1 into our UWB radar system. However, when we tested the new pulser configuration we were still unable to find any radar returns. The data shown in the Figure 7.13 is typical. We processed it by aligning it in time with the background signal, subtracting the background signal, and filtering to remove high-frequency noise. As the figure shows, we are unable to reliably identify the corner reflector returns.

We consider now the reason for our difficulties with the ASG1 with IFN. We have eliminated the limiters, so they cannot be causing the problem by limiting the return data. Because we were able to identify the returns using the fast-risetime PSPL 4015C pulse generator, we suspect that the risetime of the ASG1 is simply too slow for the corner reflector return, which tends to reflect higher frequencies better. We suspect that the ASG1 would work better with a scatterer that resonates at a lower frequency, and is placed at a larger distance from the antenna.

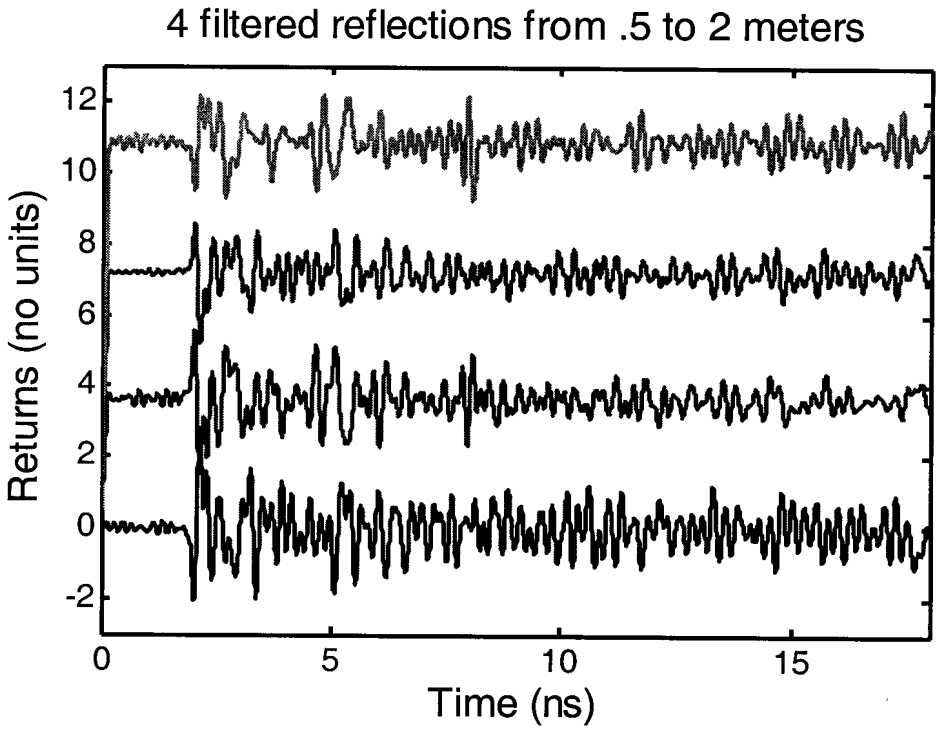

Figure 7.13. Data containing signal returns from corner reflector. (No reflections are apparent.)

8. Conclusions and Recommendations

As a first step in building a UWB radar with a single antenna, we have demonstrated the feasibility of a high-voltage UWB directional coupler based on coupled-lines. Low-voltage experimental results for two coupler designs are in reasonable agreement with our predictions. The couplers were designed for 50 kV, but were tested only at low voltage.

We have also demonstrated the use of the directional coupler in an impulse radar. Very clear reflections were apparent in the data when we used the Picosecond Pulse Lab model 4015C source. However, no reflections were apparent with the Kentech model ASG1 source, even when we used an IFN to take the derivative of the source.

Improvements can be made to the directional coupler with careful attention to high-frequency design. In particular, the transitions between coaxial input and coupled-lines could be made more smooth. Note that we designed the directional couplers to optimize their high-voltage performance, while accepting some compromises in their high frequency capability. Smoothing the impedance discontinuities of the directional couplers will increase the system's ability to resolve returns. In addition, the center conductors could be separated, to reduce losses due to finite conductivity.

Besides improving the directional coupler, there are a number of other ways to improve the performance of the radar system. First, we will see better performance as the scatterer is moved further from the antenna and as a higher voltage pulser is used. Second, we note that the corner reflector is responsive to higher frequencies than the intended target of conducting cylinders. As we test devices that are more responsive to slower waveforms, performance should improve.

Acknowledgements

We wish to thank the Air Force Research Laboratory Directed Energy Directorate for funding this work. We also wish to thank Dr. Carl E. Baum for many helpful discussions on this work.

References

1. C. E. Baum, Coupled Transmission Lines as a Time-Domain Directional Coupler, Sensor and Simulation Note 451, October 2000.

2. D. M. Pozar, *Microwave Engineering*, Second Edition, New York, John Wiley & Sons, 1998, pp. 389-394.

3. M. Piette, "Ultra-Wideband Duplexers for Low and High Peak Power Applications," pp. 187-193 in *Ultra-Wideband, Short-Pulse Electromagnetics 4* (E. Heyman, B. Mandelbaum and J. Shiloh eds.) , New York, Kluwer Academic, 1999.